


## Emergence of a Multiferroic Half-Metallic Phase in $\text{Bi}_2\text{FeCrO}_6$ through Interplay of Hole Doping and Epitaxial Strain

Paresh C. Rout<sup>1</sup> and Varadharajan Srinivasan<sup>1,2</sup>

<sup>1</sup>*Department of Physics, Indian Institute of Science Education and Research Bhopal, Bhopal 462 066, India*

<sup>2</sup>*Department of Chemistry, Indian Institute of Science Education and Research Bhopal, Bhopal 462 066, India*

 (Received 6 September 2018; revised manuscript received 17 July 2019; published 5 September 2019)

Epitaxial strain has been shown to drive structural phase transitions along with novel functionalities in perovskite-based thin films. Aliovalent doping at the *A* site can drive an insulator-to-metal and magnetic transitions in perovskites along with a variety of interesting structural and electronic phenomena. Using first-principles calculations, we predict the formation of a multiferroic half-metallic phase with a large magnetic moment in the double perovskite,  $\text{Bi}_2\text{FeCrO}_6$ , by coupling epitaxial strain with *A*-site hole doping. We also demonstrate that epitaxial strain can be used to manipulate the hole states created by doping to induce half-metal to insulator, antipolar to polar, antiferromagnetic to ferromagnetic, orbital ordering and charge ordering transitions. Our work also suggests that hole doping under strain could lead to mitigation of issues related to antisite defects and lowered magnetization in thin films of the material.

DOI: [10.1103/PhysRevLett.123.107201](https://doi.org/10.1103/PhysRevLett.123.107201)

Perovskites (with molecular formula  $\text{ABO}_3$ ) have emerged as promising candidates for multiferroicity [1–5]. Of particular interest are magnetoelectric multiferroics, where the transition metal (*B*) sites contribute to the magnetic moment while the ferroelectricity is usually associated with polar distortions induced by the *A*-site cations. These oxides are typically antiferromagnetic (AFM) Mott insulators, thereby possessing very low magnetization [3,6]. In the so-called double perovskites, where TM ions with dissimilar magnetic moments occupy *B* sites, the magnetization can be increased through ferrimagnetism while retaining ferroelectricity and magnetoelectric coupling. A prominent example of this approach is  $\text{Bi}_2\text{FeCrO}_6$  (BFCO) which was predicted to be a bulk multiferroic with a magnetic moment of  $2 \mu_B$  per formula unit [7] corresponding to a *G*-type AFM spin ordering.

In practice, multiferroic oxides are often grown as epitaxial thin films on oxide substrates. Epitaxial strain has been shown to drive structural phase transitions in thin films, stabilize magnetic states [8], induce polar-to-non-polar transitions in layered oxides [9], and significantly influence ferroic properties of thin films [10–13]. Recently, we have shown that, epitaxially grown (001) oriented BFCO thin films are unstable to antisite defects and prefer a *C*-type AFM (*C*-AFM) ordered ground state [14], both features leading to loss of magnetization [15,16]. The antisite defects basically occur due to the similarity of charge and ionic radii of  $\text{Fe}^{3+}$  and  $\text{Cr}^{3+}$  ions.

Aliovalent chemical doping in complex oxides is another practical route for controlling many properties such as structure, magnetism, magnetic transition temperature, polarization, and transport properties [17–22]. Particularly, doping in the Mott regime directly changes

the valence state of the transition metal ion (e.g., manganese) while doping in the extreme of the charge transfer regime (e.g., cuprates) results in the formation of holes on the oxygen lattice [23,24].

In this Letter, we explore aliovalent doping of BFCO thin films in conjunction with epitaxial strain as a plausible route to recover multiferroic properties and encode interesting functionalities. We found that mixing in  $\text{Sr}^{2+}$  ions at the  $\text{Bi}^{3+}$  sites in BFCO, a Mott insulator, primarily affected the valence states of the TM ions [25]. This in turn led to differing ionic sizes at the *B* sites, reducing the likelihood of cation disorder, thereby increasing the magnetization. Furthermore, changes in the oxidation state of the Cr atom also resulted in charge disproportionation (CD) and half-metallicity. Epitaxial strain played the role of stabilizing these phases, under different doping concentrations, as well as driving half-metal to insulator (HMIT) and antipolar to polar (AP-P) transitions. The combined effects of strain and doping resulted in a novel and technologically significant ferroelectric half-metal (FEHM) phase in BFCO.

Our density functional theory (DFT + *U*) based methodology, detailed in the Supplemental Material (SM) [26], consisted of strained bulk calculations on a 20-atom supercell [14] of BFCO. Biaxial strain in the *ab* plane of the supercell was varied in a range  $-4\% \leq \epsilon \leq 4\%$  to mimic cubic substrates, keeping the pseudocubic bulk BFCO as reference. For each such strain, the out-of-plane parameter, the monoclinic angle ( $\beta$ ) and all internal coordinates were fully relaxed.  $\text{Bi}_{2-x}\text{Sr}_x\text{FeCrO}_6$  (SBFCO) was modeled by replacing one ( $x = 0.5$ ) and two ( $x = 1$ ) Bi ions by Sr, respectively. Having considered various *B*-site cation orderings possible within the 20-atom supercell for relaxation calculations, we focused on two energetically

important ones: the rock-salt ordered structure ( $D0$ ) and a structure with layers of Fe and Cr alternating in the (001) direction ( $D1$ ). In each case, we considered four types of magnetic ordering: AFM ( $A$ ,  $C$ ,  $G$ -type) and the FM orders (see SM [26], Fig. 2). Additionally, the structures conformed to  $P2_1/n$  (antipolar) and  $R3$  (polar) space groups, respectively, as these were lowest in energy (see SM [26]) and also compatible with cubic substrates [47,48]. These essentially differ by the sense and relative magnitudes of oxygen octahedral rotations as indicated by the Glazer notation  $a^-a^-c^+$  and  $a^-a^-a^-$ , respectively.

Undoped BFCO thin films are not only susceptible to antisite defects under all epitaxial strains [14], but also result in  $C$ -AFM ground state regardless of the cation ordering (see SM [26], Fig. 23). Figure 1 shows the relative energies of the lowest lying states as a function of epitaxial strain in SBFCO. The immediate effect of hole doping is the stabilization of the rock-salt ordered  $D0$  structure along with the realization of the FM ground state with a large moment of  $7.5 \mu_B/\text{f.u.}$  Epitaxial strain further induces AP-P and FM to AFM transitions.

The  $D0$   $R3$  phase undergoes an isosymmetric phase transition (IPT) [49–52] at  $\approx 2\%$  characterized by symmetry-preserving reorientation of octahedra. The resulting phase, referred to as  $R3(1)$  below, emerges as the most stable phase at 4% strain. Similar IPTs also occur at  $-2\%$  strain in the  $D0$   $R3$  phase and at 0% strain in the  $D0$   $P2_1/n$  structure (see also SM [26], Fig. 6). These IPTs are also indicated by sudden changes in the average oxygen octahedral tilt (OOT) and rotation (OOR) angles [53] in

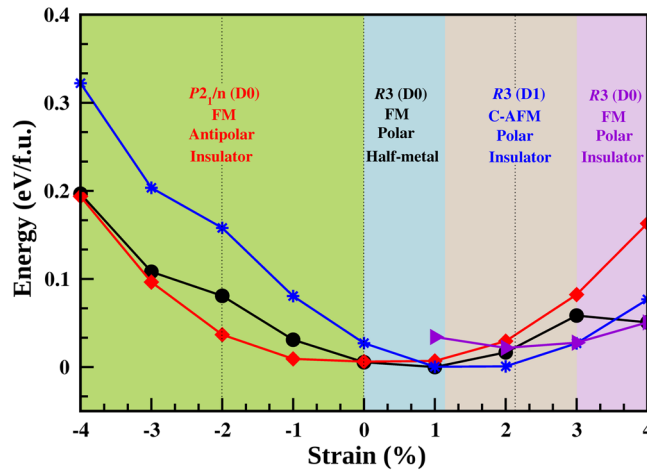


FIG. 1. Total energy difference (in eV per formula unit) as a function of epitaxial strain in the three lowest energy phases of  $\text{BiSrFeCrO}_6$ : black circles represent the FM state of  $D0$  structure in  $R3$  phase, red diamonds, the FM state of  $D0$  structure in  $P2_1/n$ -phase, and blue asterisks, the  $C$ -AFM state of  $D1$  structure in  $R3$  phase. The indigo triangles represent the FM state of  $D0$  structure in  $R3(1)$  phase which occurs as a result of an IPT at 2% strain. The dotted vertical lines indicate the locations of the isosymmetric phase transition (IPT).

the  $D0$  structure, as shown in Fig. 2(a), for both  $P2_1/n$  as well as  $R3$  phases.

The stabilization of FM ordering in the  $D0$  structure upon 50% hole doping is most directly an effect of the increase of Fe-O-Cr superexchange angles beyond  $150^\circ$  throughout all strains. It has been shown, previously [14], that the  $\text{Fe}^{3+}\text{-Cr}^{3+}$  ( $d^5-d^3$ ) superexchange coupling switches from AFM to FM beyond this critical angle. The introduction of the larger  $\text{Sr}^{2+}$  ions at the  $A$  site leads to lesser tilts in the oxygen octahedra and, hence, larger Fe-O-Cr angles. Additionally, the hole doping results in an oxidation of the Cr site to a  $d^2$  configuration further strengthening an FM superexchange interaction [54–56] between Fe and Cr. In the  $R3$   $D1$  structure (1.2–2.8% strain), the out-of-plane Fe-Cr interactions become FM due to increased superexchange angles ( $\sim 157^\circ$ ), but the in-plane interactions between like ions (Cr-Cr and Fe-Fe) are AFM, as expected [54], resulting in a  $C$ -AFM ground state in this region of strain. Hence, the FM to AFM transition at  $\sim 1\%$  strain is induced by the  $B$ -site cation ordering transition.

We used the  $A$ -site ion displacement (relative to the ideal structure), along the pseudocubic [110] direction, as an order parameter to follow the effect of hole doping on the polarization in BFCO [7,51,57]. These are plotted in Fig. 2(b) for the most stable phases at each strain. A clear AP-P transition is seen at 0% strain where the Bi and Sr displacements of SBFCO go from being antiparallel to each other to moving in the same direction. This is consistent with the change of space-group from  $P2_1/n$  to  $R3$  at 0% strain. Thus, an AP-P transition is induced by epitaxial strain upon hole doping. The polar phase survives the cation reordering transition at 1.2%, thereby dominating the entire tensile strain region.

Figure 3 shows the density of states projected on the Cr  $3d$  and O  $2p$  atomic states (PDOS) which contribute the most near the Fermi energy (see SM [26], Fig. 9 for PDOS in a wider range of energies). Hole doping and epitaxial strain directly affect the Cr  $t_{2g}$  orbitals which are strongly hybridized with the O  $2p$  orbitals. In the compressive strain region, the  $d_{xy}$  orbital is destabilized and splits off from the  $t_{2g}$  triplet, appearing as the narrow hole band in Fig. 3(a). The other two orbitals in the triplet remain nearly degenerate and are each singly occupied resulting in a  $\text{Cr}^{4+}$  ion with a moment of  $\sim 2 \mu_B$ . Thus, the  $D0$  FM  $P2_1/n$  phase becomes insulating with a narrow gap of  $\sim 0.1$  eV.

With reducing compressive strain, the degeneracy of the three  $t_{2g}$  levels is gradually restored, turning the system metallic and giving rise to a HMIT at 0% strain. At the transition point, there is also a charge transfer from the O  $2p$  to the Cr  $3d$  giving the hole a dominant O  $2p$  character [see Fig. 3(b)]. Thus, epitaxial strain pushes the hole-doped system to a negative charge transfer regime [58,59]. Coincidentally, there is also a structural change from the  $P2_1/n$  to the  $R3$  phase at this strain. The HM  $R3$

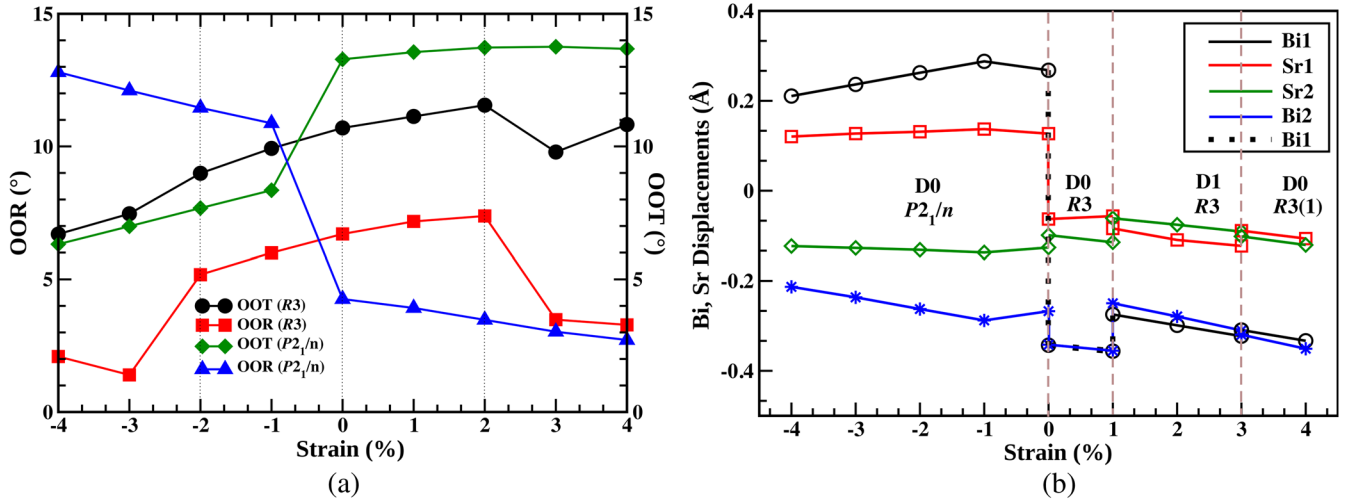


FIG. 2. (a) The average oxygen octahedral rotation (OOR) and oxygen octahedral tilt (OOT) angles as a function of biaxial strain for all the stable phases. The IPTs (indicated by vertical dotted lines) are characterized by sharp changes in the OOT and OOR in the antipolar ( $P2_1/n$ ) phase at 0% strain and in the polar ( $R3$ ) phase at  $-2\%$  and  $+2\%$  strain; and (b) The Bi, Sr displacements (in Å), along the pseudocubic  $[110]$  direction, from their respective positions in the ideal perovskite structure: open black circles (as well as the dotted black line) represent Bi1 displacements, blue asterisks, Bi2 displacements, open red squares and green diamonds, Sr1 and Sr2 displacements, respectively, where 1 and 2 refer to the two planes of  $A$  sites in the supercell. The vertical dashed lines separate the various phases identified in 1.

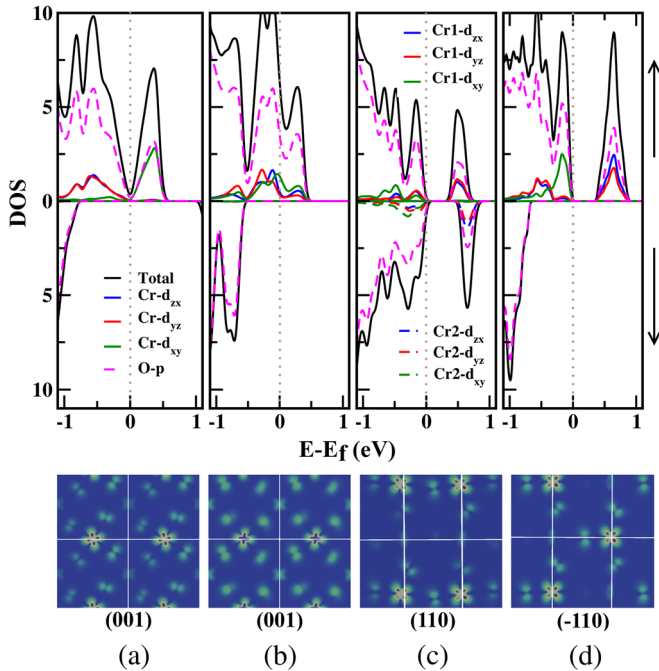


FIG. 3. Total and projected density of states (PDOS) of lowest energy phases of  $\text{BiSrFeCrO}_6$  at various strains (top panel) and the spatial distribution of the corresponding hole states (bottom panel) on selected planes (indicated below the figures). (a) The antipolar ( $P2_1/n$ )  $D0$  phase at  $-4\%$  strain; (b) the polar ( $R3$ )  $D0$  phase at 0% strain, (c) the polar ( $R3$ )  $D1$  phase at  $+2\%$  strain (Cr1 and Cr2 refer to the two spin inequivalent Cr atoms in the system); and (d) the isosymmetric polar ( $R3(1)$ )  $D0$  phase at  $+4\%$ .

phase, which extends over a narrow strain region (0–1.2%) and has an FM ordered ground state due to the same reasons as the  $P2_1/n$  phase at compressive strain. The concurrence of half-metallicity and polar nature is, however, a surprise. Sustaining polarization in a metal has been considered unlikely because of screening by conduction electrons, making such materials rare. While polar metals have been shown to exist [60,61], there is no previous report of the FEHM state. In such a material, spin-selective screening effects could stabilize an electrically polarized state, with dominant contribution to the polarization arising from the one-spin channel. This property would be extremely appealing for spintronics device applications and is currently under investigation.

The cation-ordering transition seen at 1.2% strain also coincides with a HMIT [see Fig. 3(c)]. Once again, there is a clear splitting of the Cr  $t_{2g}$  levels, but this time, the hole state corresponds to a linear combination of the  $d_{xz}$  and  $d_{yz}$  orbitals [62,63]. Another linear combination of these orbitals is below the Fermi level along with the  $d_{xy}$  level. The layered nature of the phase leads to an AFM interaction between the Cr ions resulting in the  $C$ -AFM ordering. The hole state is localized on the Cr and nearby oxygens and is distributed mostly in a plane parallel to (110). Interestingly, at larger strains ( $> 2.8\%$ ), where the polar  $D0$  phase reemerges as the most stable phase  $R3(1)$ , the same disposition of the  $d$  orbitals survives. Hence, the HM nature of the polar  $D0$  phase vanishes and we get an insulating ground state with a narrow band gap [see Fig. 3(d)]. The overall effect of strain is to generate orbitally ordered states

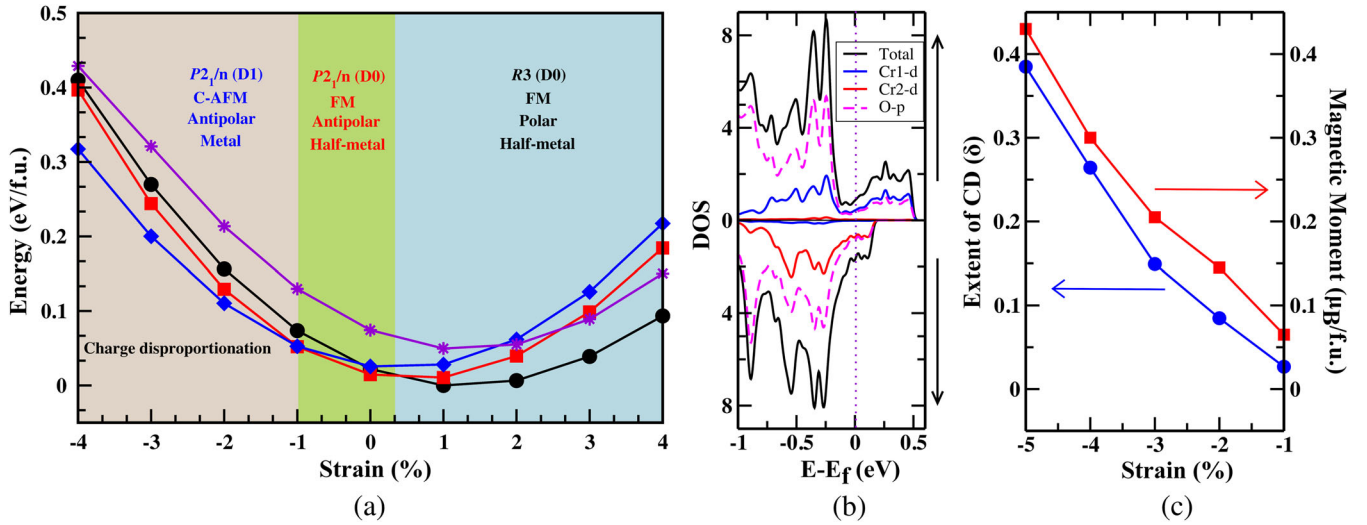


FIG. 4. Epitaxial strain induced phase transitions in  $\text{Bi}_{1.5}\text{Sr}_{0.5}\text{FeCrO}_6$ . (a) Evolution of total energy (in eV per formula unit) with epitaxial strain in the three lowest energy phases: black circles represent the FM state of  $D0$   $R3$  structure, red squares, the FM state of  $D0$  structure  $P2_1/n$  structure, and blue diamonds, the  $C$ -AFM state of  $D1$  structure  $P2_1/n$  structure. The energy of the  $C$ -AFM state of  $D1$  structure in  $R3(1)$  phase, which was stable at 50% doping, is also presented (indigo asterisks) for purposes of comparison. All the energies are positioned with respect to the energy of the  $D0$  FM ( $R3$ ) state at 1% strain, (b) Total and projected density of states (PDOS) of the antipolar ( $P2_1/n$ ) phase of  $D1$  structure at  $-4\%$  strain, and (c) The atomic charge difference between the two types of Cr atoms (Cr1 and Cr2) and magnetic moment per formula unit of  $C$ -AFM  $D1$  structure as a function of compressive strain.

as shown in the bottom panel of Fig. 3, where the integrated local density of states arising from the hole bands is plotted. From compressive to tensile strain, the hole state continuously changes from being on the (001) plane to a perpendicular plane. Thus, strain drives an orbital reordering transition that goes through the half-metallic state at 0% with no orbital ordering (degenerate  $t_{2g}$  levels). The IPT (originating at 2%), driven by symmetry-preserving oxygen octahedral reorientations, leads to the HM in the polar  $D0$  structure.

The FEHM phase, although interesting, is only stable in a narrow strain window. Its stability can be enhanced by varying the stoichiometric percentage of Sr. A smaller Sr doping would also make CD possible at the Cr sites and could lead to charge-ordering (CO). Hence, we calculated the epitaxial strain driven phase diagram of 25% doped BFCO shown in Fig. 4. In the compressive strain region (i.e.,  $-4\%$  to  $-1.0\%$  strain) the  $C$ -AFM layered  $D1$  structure becomes stable, as in the case of the pure BFCO, but is antipolar. However, between  $-1.0\%$  and  $0.4\%$  strain, the antipolar FM phase becomes stable. Most surprisingly, the FEHM phase is stabilized in a wide range of tensile strain. The HM nature was confirmed by calculating its density of states (see SM [26], Fig. 22). Thus, epitaxial strain drives both magnetic ordering and structural transitions at 25% Sr doping. However, we did not observe any strain-driven IPT in this case. Even with 25% Sr doping, the cation ordered  $D0$  structure is stabilized under a wide range of epitaxial strain while retaining a large magnetization through a FM ordered ground state.

Interestingly, we observed that, under compressive strain, the ground-state layered structure yields a small nonzero magnetic moment ( $\sim 0.5 \mu_B/\text{f.u.}$ ) and is metallic despite an overall  $C$ -AFM ordering of the spins. Furthermore, this magnetic moment increases with compressive strain [see Fig. 4(c)] correlating well with an increase in the charge difference between the two Cr sites in the layer. This is indicative of CD in the Cr sublattice to  $\text{Cr}^{3.5+\delta}$  (Cr1) and  $\text{Cr}^{3.5-\delta}$  (Cr2), respectively. At higher compressive strain, the extent of CD ( $\delta$ ) increases with the ions tending towards  $4+$  ( $t_{2g}^2 e_g^0$ ) and  $3+$  ( $t_{2g}^3 e_g^0$ ) oxidation states, respectively. The CD is also confirmed by the PDOS [see Fig. 4(b)] for the system where the two Cr atoms are seen to be clearly inequivalent, not only having opposite spins, but also contributing differently at the Fermi level. With increasing compressive strain, the octahedral volume at Cr1 decreases much faster than that at Cr2, clearly indicating that the former has a larger charge (see SM [26], Figs. 20 and 21). The measured magnetic moment of  $0.43 \mu_B/\text{f.u.}$  at  $-4\%$  strain is consistent with the proposed CD and the fact that the Fe ions are unaffected ( $\text{Fe}^{3+}: t_{2g}^3 e_g^2$ ) by the doping. The localization of the hole on the Cr layer leads to a checker-board patterned CO in the 20-atom supercell considered.

Both the antipolar ( $P2_1/n$ )  $D0$  phase and the polar ( $R3$ )  $D0$  phase are HM as indicated by their PDOS (see SM [26], Fig. 22). Both phases have FM ordering with a total spin magnetic moment of  $7.5 \mu_B/\text{f.u.}$  The Fe atoms retain their formal oxidation state of  $3+$  ( $t_{2g}^3 e_g^2$ ), whereas the Cr atoms

are equally divided between 4+ and 3+ oxidation states, with the hole localized on the Cr atom closest to the Sr atom. While the FM state has been realized in other Bi-based multiferroics previously [64], this is the highest magnetic moment predicted in Bi-based double perovskites so far.

In summary, the interplay of the hole-doping and epitaxial strain in BFCO results in not only recovering ferroic properties, but also a rich phase diagram. The added holes localize on the Cr sublattice resulting in competing effects of correlation and structural distortions as anticipated in other systems [62,63,65]. The epitaxially strained Sr-doped film is able to host almost all the anticipated orders connected to each other by strain-induced phase transitions. The most interesting observation was the stabilization of a FEHM with a large magnetic moment state in a narrow tensile strain window. The stability range of this phase is significantly enhanced at lower doping concentration. The multiferroic HM phase we have predicted is certain to attract much attention in the near future [66,67]. Furthermore, the hole-induced stabilization of the rock-salt ordered structure under most strains could likely indicate suppression of antisite defects in BFCO. We anticipate that the SBFCO structure can be readily formed in experiments as indicated by favorable tolerance factors as well as the fact that thin films of the parent compound have already been formed. We hope that our observations will initiate further experimental efforts to verify the interesting predictions made in this work.

The authors would like to thank Mr. Shashi Saurav and all the AITG group members at IISER, Bhopal for their help and invaluable discussion. The authors gratefully acknowledge IISER Bhopal for computational resources and funding. P. C. R. would like to acknowledge CSIR for funding through the Junior Research Fellowship Programme.

---

[1] W. Eerenstein, N. D. Mathur, and J. F. Scott, *Nature (London)* **442**, 759 (2006).  
 [2] S. Cheong and M. Mostovoy, *Nat. Mater.* **6**, 13 (2007).  
 [3] R. Ramesh and N. A. Spaldin, *Nat. Mater.* **6**, 21 (2007).  
 [4] J. Van Den Brink and D. I. Khomskii, *J. Phys. Condens. Matter* **20**, 434217 (2008).  
 [5] J. Ma, J. Hu, Z. Li, and C.-W. Nan, *Adv. Mater.* **23**, 1062 (2011).  
 [6] C. Ederer and N. A. Spaldin, *Phys. Rev. B* **71**, 224103 (2005).  
 [7] P. Baettig, C. Ederer, and N. A. Spaldin, *Phys. Rev. B* **72**, 214105 (2005).  
 [8] D. Meng, H. Guo, Z. Cui, C. Ma, J. Zhao, J. Lu, H. Xu, Z. Wang, X. Hu, Z. Fu *et al.*, *Proc. Natl. Acad. Sci. U.S.A.* **115**, 2873 (2018).  
 [9] X.-Z. Lu and J. M. Rondinelli, *Nat. Mater.* **15**, 951 (2016).  
 [10] J. H. Lee *et al.*, *Nature (London)* **466**, 954 (2010).

[11] J. H. Lee and K. M. Rabe, *Phys. Rev. Lett.* **104**, 207204 (2010).  
 [12] H. Chen and A. J. Millis, *Phys. Rev. B* **94**, 165106 (2016).  
 [13] D. G. Schlom, L.-Q. Chen, C. J. Fennie, V. Gopalan, D. A. Muller, X. Pan, R. Ramesh, and R. Uecker, *MRS Bull.* **39**, 118 (2014).  
 [14] P. C. Rout, A. Putatunda, and V. Srinivasan, *Phys. Rev. B* **93**, 104415 (2016).  
 [15] V. Shabadi, M. Major, P. Komissinskiy, M. Vafae, A. Radetinac, M. Baghaie Yazdi, W. Donner, and L. Alff, *J. Appl. Phys.* **116**, 114901 (2014).  
 [16] G. Vinai, A. Khare, D. S. Rana, E. Di Gennaro, B. Gobaut, R. Moroni, A. Y. Petrov, U. Scotti di Uccio, G. Rossi, F. Mileto Granozio, G. Panaccione, and P. Torelli, *APL Mater.* **3**, 116107 (2015).  
 [17] H. Y. Hwang, S.-W. Cheong, P. G. Radaelli, M. Marezio, and B. Batlogg, *Phys. Rev. Lett.* **75**, 914 (1995).  
 [18] J. Navarro, C. Frontera, L. Balcells, B. Martínez, and J. Fontcuberta, *Phys. Rev. B* **64**, 092411 (2001).  
 [19] H. Tsukahara, S. Ishibashi, and K. Terakura, *Phys. Rev. B* **81**, 214108 (2010).  
 [20] D. Serrate, J. De Teresa, J. Blasco, M. Ibarra, L. Morellón, and C. Ritter, *Appl. Phys. Lett.* **80**, 4573 (2002).  
 [21] N. Zu, J. Wang, Y. Wang, and Z. Wu, *Dalton Trans.* **43**, 8698 (2014).  
 [22] J. Fujioka, S. Miyasaka, and Y. Tokura, *Phys. Rev. B* **72**, 024460 (2005).  
 [23] M. Imada, A. Fujimori, and Y. Tokura, *Rev. Mod. Phys.* **70**, 1039 (1998).  
 [24] S. Medling, Y. Lee, H. Zheng, J. F. Mitchell, J. W. Freeland, B. N. Harmon, and F. Bridges, *Phys. Rev. Lett.* **109**, 157204 (2012).  
 [25] H. S. Lee, S. G. Choi, H.-H. Park, and M. J. Rozenberg, *Sci. Rep.* **3**, 1704 (2013).  
 [26] See Supplemental Material at <http://link.aps.org/supplemental/10.1103/PhysRevLett.123.107201> for details of methodology, supporting data, and analyses, which includes Refs. [27–46].  
 [27] P. Giannozzi *et al.*, *J. Phys. Condens. Matter* **21**, 395502 (2009).  
 [28] J. P. Perdew, K. Burke, and M. Ernzerhof, *Phys. Rev. Lett.* **77**, 3865 (1996).  
 [29] J. P. Perdew, K. Burke, and M. Ernzerhof, *Phys. Rev. Lett.* **78**, 1396 (1997).  
 [30] V. I. Anisimov, F. Aryasetiawan, and A. I. Liechtenstein, *J. Phys. Condens. Matter* **9**, 767 (1997).  
 [31] M. Cococcioni and S. de Gironcoli, *Phys. Rev. B* **71**, 035105 (2005).  
 [32] B. Himmetoglu, R. M. Wentzcovitch, and M. Cococcioni, *Phys. Rev. B* **84**, 115108 (2011).  
 [33] A. Glazer, *Acta Crystallogr. Sect. A* **31**, 756 (1975).  
 [34] A. Glazer, *Acta Crystallogr. Sect. B* **28**, 3384 (1972).  
 [35] P. M. Woodward, *Acta Crystallogr. Sect. B* **53**, 32 (1997).  
 [36] R. D. Shannon, *Acta Crystallogr. Sect. A* **32**, 751 (1976).  
 [37] H. P. S. Corrêa, I. P. Cavalcante, D. O. Souza, E. Z. Santos, M. T. D. Orlando, H. Belich, F. J. Silva, E. F. Medeiro, J. M. Pires, J. L. Passamai, L. G. Martinez, and J. L. Rossi, *Cerâmica* **56**, 193 (2010).  
 [38] P. Ravindran, R. Vidya, A. Kjekshus, H. Fjellvåg, and O. Eriksson, *Phys. Rev. B* **74**, 224412 (2006).

- [39] H. J. Xiang, *Phys. Rev. B* **90**, 094108 (2014).
- [40] P. S. Wang, W. Ren, L. Bellaïche, and H. J. Xiang, *Phys. Rev. Lett.* **114**, 147204 (2015).
- [41] K. Gupta, P. Mahadevan, P. Mavropoulos, and M. Ležaić, *Phys. Rev. Lett.* **111**, 077601 (2013).
- [42] H. T. Dang, X. Ai, A. J. Millis, and C. A. Marianetti, *Phys. Rev. B* **90**, 125114 (2014).
- [43] J. H. Lee and K. M. Rabe, *Phys. Rev. Lett.* **107**, 067601 (2011).
- [44] J.-S. Zhou, C.-Q. Jin, Y.-W. Long, L.-X. Yang, and J. B. Goodenough, *Phys. Rev. Lett.* **96**, 046408 (2006).
- [45] Z. Li, T. Itaka, and T. Tohyama, *Phys. Rev. B* **86**, 094422 (2012).
- [46] J. M. Perez-Mato, D. Orobengoa, and M. I. Aroyo, *Acta Crystallogr. Sect. A* **66**, 558 (2010).
- [47] A. Khare, A. Singh, S. S. Prabhu, and D. S. Rana, *Appl. Phys. Lett.* **102**, 192911 (2013).
- [48] R. Nechache, C. Harnagea, A. Ruediger, F. Rosei, and A. Pignolet, *Funct. Mater. Lett.* **3**, 83 (2010).
- [49] R. Zeches, M. Rossell, J. Zhang, A. Hatt, Q. He, C.-H. Yang, A. Kumar, C. Wang, A. Melville, C. Adamo *et al.*, *Science* **326**, 977 (2009).
- [50] A. J. Hatt, N. A. Spaldin, and C. Ederer, *Phys. Rev. B* **81**, 054109 (2010).
- [51] J. M. Rondinelli and S. Coh, *Phys. Rev. Lett.* **106**, 235502 (2011).
- [52] A. G. Christy, *Acta Crystallogr. Sect. B* **51**, 753 (1995).
- [53] A. T. Zayak, X. Huang, J. B. Neaton, and K. M. Rabe, *Phys. Rev. B* **74**, 094104 (2006).
- [54] J. Goodenough, *Phys. Rev.* **100**, 564 (1955).
- [55] J. Kanamori, *J. Phys. Chem. Solids* **10**, 87 (1959).
- [56] E. O. Wollan, *Phys. Rev.* **117**, 387 (1960).
- [57] L. Bellaïche and J. Íñiguez, *Phys. Rev. B* **88**, 014104 (2013).
- [58] D. Khomskii, [arXiv:cond-mat/0101164](https://arxiv.org/abs/cond-mat/0101164).
- [59] J. Zaanen, G. A. Sawatzky, and J. W. Allen, *Phys. Rev. Lett.* **55**, 418 (1985).
- [60] T. H. Kim, D. Puggioni, Y. Yuan, L. Xie, H. Zhou, N. Campbell, P. J. Ryan, Y. Choi, J.-W. Kim, J. R. Patzner, S. Ryu, J. P. Podkaminer, J. Irwin, Y. Ma, C. J. Fennie, M. S. Rzchowski, X. Q. Pan, V. Gopalan, J. M. Rondinelli, and C. B. Eom, *Nature (London)* **533**, 68 (2016).
- [61] D. Puggioni and J. M. Rondinelli, *Nat. Commun.* **5**, 3432 (2014).
- [62] A. C. Komarek, S. V. Streltsov, M. Isobe, T. Möller, M. Hoelzel, A. Senyshyn, D. Trots, M. T. Fernández-Díaz, T. Hansen, H. Gotou, T. Yagi, Y. Ueda, V. I. Anisimov, M. Grüninger, D. I. Khomskii, and M. Braden, *Phys. Rev. Lett.* **101**, 167204 (2008).
- [63] H.-S. Jin, K.-H. Ahn, M.-C. Jung, and K.-W. Lee, *Phys. Rev. B* **90**, 205124 (2014).
- [64] M. Azuma, K. Takata, T. Saito, S. Ishiwata, Y. Shimakawa, and M. Takano, *J. Am. Chem. Soc.* **127**, 8889 (2005).
- [65] K.-W. Lee and W. E. Pickett, *Phys. Rev. B* **80**, 125133 (2009).
- [66] P. C. Rout and V. Srinivasan, [arXiv:1807.01649](https://arxiv.org/abs/1807.01649) [Phys. Rev. Lett. (to be published)].
- [67] D. Puggioni, A. Stroppa, and J. M. Rondinelli, *Phys. Rev. Mater.* **2**, 114403 (2018).